Carbon 199 (2022) 80–86

Contents lists available at ScienceDirect

Carbon

journal homepage: www.elsevier.com/locate/carbon

Nanotribology and electrical properties of carbon nanotubes hybridized with covalent organic frameworks

Alicia Moya [a], José Alemán [b,c], Julio Gómez-Herrero [d,e], Rubén Mas-Ballesté [c,f], Pedro J. de Pablo [d,e,*]

[a] Univ. Grenoble Alpes, Univ. Savoie Mont Blanc, CNRS, IRD, IFSTTAR, ISTerre, 38000 Grenoble, France
[b] Department of Organic Chemistry, Universidad Autónoma de Madrid, 28049, Madrid, Spain
[c] Institute for Advanced Research in Chemical Sciences (IAdChem), Universidad Autónoma de Madrid, 28049, Madrid, Spain
[d] Department of Condensed Matter Physics, Universidad Autónoma de Madrid, 28049, Madrid, Spain
[e] Institute of Condensed Matter Physics (IFIMAC), Universidad Autónoma de Madrid, 28049, Madrid, Spain
[f] Department of Inorganic Chemistry, Universidad Autónoma de Madrid, 28049, Madrid, Spain

ARTICLE INFO

Keywords:
friction
Nanomanipulation
AFM
Nanotubes
Mechanical and electrical properties

ABSTRACT

Nanomanipulation of molecular materials such as carbon nanotubes (CNTs) or new covalent organic frameworks (COFs) is key not only for the study of their fundamental physicochemical properties, but also for building and probing nanodevices. Therefore, we have investigated the tribological properties of oxidized MWCNTs (ox-MWCNTs) and their hybridization with COF building blocks (ox-MWCNTs@COF) adsorbed on a mica surface. We used the AFM tip to apply torsional forces on individual nanotubes. Depending on the manipulation parameters, the lateral displacements of the AFM tip slide and/or bend nanotubes enabling the direct quantification of the nanotube-mica adhesion. We found striking changes in the behaviour of the lateral force needed to manipulate each carbon nanotube variant which indicates an increased adhesion of ox-MWCNTs@COF with respect to ox-MWCNTs (~10x). In addition, the use of the AFM tip as a mobile electrode enabled the measurement of electrical transport through individual nanotubes that revealed a rectifying behaviour of the ox-MWCNTs@COF with high resistivity, which was in contrast with the near ohmic performance of ox-MWCNTs.

1. Introduction

Carbon Nanotubes (CNTs) are considered to be a potential multifunctional material for constructing nanodevices due to their exceptional mechanical, electrical and thermal properties [1–4] which enable their use in many applications such as field emission and photovoltaic devices, batteries or supercapacitors [5–8]. These remarkable properties together with their nanomolecular construction and high surface area to volume ratio contributes to a reduction in the size and weight of materials, features which have an important impact on the industry [9]. These types of nanomaterials have attracted a huge interest due to their performance at the nanoscale which provides new insights and properties from both fundamental and applied perspectives [10–12]. When dealing with molecular nanomaterials such as CNTs, both the study of their individualized physicochemistry [13] and the manufacture of nanodevices requires their manipulation at the nanoscale [14]. This procedure involves positional modification, controlled deformation, and nano-electrical connection [15,16].

Atomic force microscopy (AFM) is often used for the nanomanipulation of single molecular objects at the nanoscale for assembly into complex nanodevices [17,18]. In this vein, the abilities of AFM constitute an attractive strategy for the construction of nanodevices with single metallic or semiconducting nanotubes or nanowires [19–21]. Various reports have manipulated individual CNTs with the AFM tip and monitored their change in position, shape or length with topographical maps at high resolution. Such topographical information has been used for theoretical calculations of strain energies and frictional forces [22–26] which can alternatively be measured during the manipulation process if registering both the normal and the torsional bending of the AFM cantilever [27–33].

CNTs can be used as molecular templates for other active components, resulting in highly engineered composite or hybrid materials [34,35]. Because these nanocarbons are chemically robust, they are usually hybridized with other molecules or materials [36]. In particular, the

* Corresponding author. Department of Condensed Matter Physics (module 03), Universidad Autónoma de Madrid, 28049, Madrid, Spain.
E-mail addresses: alicia.moya-cuenca@univ-grenoble-alpes.fr (A. Moya), ruben.mas@uam.es (R. Mas-Ballesté), p.j.depablo@uam.es (P.J. de Pablo).

https://doi.org/10.1016/j.carbon.2022.07.053
Received 13 April 2022; Received in revised form 6 July 2022; Accepted 19 July 2022
Available online 30 July 2022

hybridization of covalent organic frameworks (COFs) and nanocarbons (either CNTs or graphene) has been recently reported as an efficient way for the enhancement in their performance in various applications such as gas adsorption, electrochemical sensing, catalyst and energy storage [37–40]. Taking advantage of the self-assembling aspect of COFs on the nanotubes template, we previously reported a new hybrid material and showed enhanced resistance to fracture of oxidized multiwalled carbon nanotubes (ox-MWCNTs) coated with Covalent Organic Frameworks (ox-MWCNTs@COF) [41].

In this work, we present an optimized nanomanipulation methodology using the AFM tip in the characterization of two kinds of nanotubes: ox-MWCNTs and ox-MWCNTs@COF (Fig. 1). The choice of oxidized MWCNT was based on our previous observations in which we only obtained homogeneous CNT-COF hybrid nanotubes when oxidized nanotubes were used [41]. Here, we have slid and bent individual nanotubes adsorbed on a mica surface by lateral manipulation. These experiments have revealed a differentiated tribological behaviour for each material, which is related to the higher adhesion of ox-MWCNTs@COF. In addition, we used a conductive AFM tip as a mobile electrode for performing electrical characterization of individual ox-MWCNTs and ox-MWCNTs@COF hybrid nanotubes.

2. Experimental section

2.1. Materials

Oxidized MWCNTs were purchased from Nanocyl Ltd and used as received. They were dispersed in ethanol and mixed with the precursors of the COF-3D (tetrakis(4-amino-phenyl)methane and terephthalaldehyde). Using an acid media (adding 10 μL of acetic acid), the formation of COF material occurs on the CNT surface, which acts as a template for the nucleation of the COF particles. As result, they were conformally coated with 3D-COF (known as COF-300) as previously reported. The result was a carbon nanotube covered with a COF layer of ~12 nm [41].

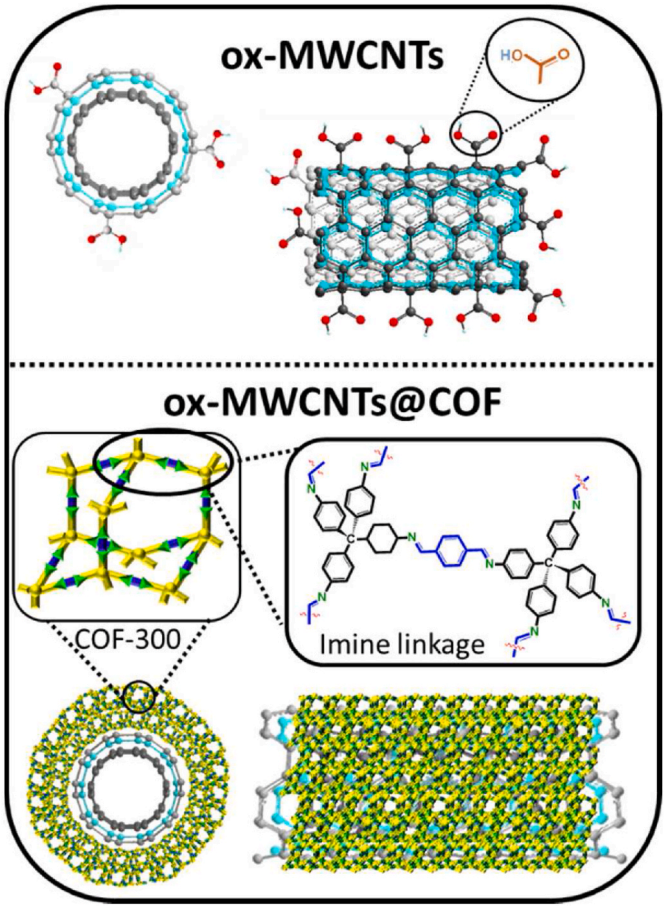

Fig. 1. Tubes used in the experiments. Scheme of oxidized multiwalled carbon nanotubes referred as ox-MWCNTs (top) and their coating with a COF layer (referred as ox-MWCNTs@COFs), formed by imine linkage between organic building blocks (amine and aldehyde).

2.2. Nanomanipulation experiments

The AFM was operated in both dynamic [42] and contact modes for imaging and manipulation, respectively. The AFM was housed inside a temperature-controlled chamber (18 °C) to ensure thermal stability. The nanomanipulation experiments were carried out using rectangular silicon nitride AFM cantilevers (RC800PSA, Olympus, Tokyo, Japan) with a nominal spring constant of 0.35 N/m that were routinely calibrated using Sader's method [43]. A Si grating was used to calibrate the torsional force (Supplementary Material -SI-) For the nanomanipulation of the nanotubes, a script was developed in WSxM software [44] to draw a path line, through which the AFM tip would be moved at constant speed with a preselected normal loading (SI). We recorded simultaneous lateral and normal forces *vs.* piezo displacement curves for the perpendicular and lateral excursions. In order to monitor the position of the nanotubes we took AFM topography images before and after each manipulation using WSxM software [44] for data and image processing. 10 μL of the sample solution (1 % wt. in ethanol) was sonicated for 1 h and incubated on the surface. The non-adsorbed particles and contaminants were removed by drying the sample with N_2.

2.3. Conductance experiments

For conductance AFM measurements, cantilevers with an electrically conductive coating of Cr–Pt were used (ElectriMulti75-G, BudgetSensors) with a nominal length of 225 μm, a width of 28 μm and a thickness of 3 μm. The cantilever spring constant was calibrated using Sader's method (3 N/m). The nominal diameter of the tip was <25 nm. The force and current *vs.* distance curves were simultaneously recorded for the forward and backward directions. In addition, images were acquired before and after the conductance measurements. For adsorption of the carbon nanotubes, 10 μL of the sample dispersion (1 % wt. in ethanol, sonicated for 1 h) were incubated on a silicon surface where Ti/Au electrodes were pre-patterned for electrical contact. The minute Ti/Au electrodes were micro-welded to a print circuit board (PCB) that was connected to the source bias voltage (Fig. 6). Most of the non-adsorbed particles were removed by drying the sample with N_2. Although we carefully protected the substrate to avoid the capture of any contaminants during the material deposition, non-adsorbed contaminants could be also removed when drying with N_2 gas. In fact, it is important to mention that we did not observed contamination could interfere with our experiments. Finally, the nanotubes connected to the electrode on one side were electrically contacted with a conductive AFM tip on the other side.

3. Results and discussion

3.1. Lateral force calibration

In order to quantify the data obtained when the AFM tip was dragged onto the surface to move the individual nanotubes, it was necessary to calibrate the torsional stiffness. Although several methodologies are available [45,46] the dragging of carbon nanotubes on surfaces is not usually calibrated [19,33,47,48]. Firstly, the lateral spring constant K_L can be simply calculated using the equation [49]:

$$K_N \Big/ K_L = 1 \Big/ 2(h/l)^2 \quad (1)$$

where: K_N and K_L are the normal and lateral spring constants, h the tip height and l the length of the cantilever [50]. The lateral spring constant obtained resulted in a value of $K_L \sim$ 690–830 N/m. Using a commercially available step grating sample (TGZ1) [51], we repeatedly scanned its steps and observed an abrupt change in the lateral force curves (Figs. S1 and SI). From the slope of these curves, we calculated a lateral force sensitivity of the AFM cantilever of 22 ± 1 mV/nm (Fig. S1E), which converts the photodiode lateral signal voltage V_L to the torsional force F_L (N).

3.2. Optimization of parameters for lateral manipulations

It was convenient to use the same surface support to enable a direct comparison between the two types of CNTs. In addition, it was important to avoid using surfactants, such as sodium dodecylsulfate [52] that could influence the adsorption and subsequent tribology of the CNTs. After exploring several options, we chose mica because nanotubes adsorption occurred in the absence of surfactant.

Once the lateral output was calibrated, we changed the sample to adsorbed ox-MWCNTs on a mica surface. AFM was used in the dynamic mode for imaging, by oscillating the tip at the cantilever resonance frequency and engaging the feedback at the amplitude (amplitude modulation) [42]. In order to perform lateral force curves, we developed a script in the lithography mode of WSxM software [44] (SI). We first moved the tip to the origin of the manipulation path and deactivated both the driving force and feedback loop of the cantilever. Then, the tip was brought to the surface until a certain normal force was reached (Fig. 2A1). Subsequently, the tip was laterally moved at a preselected velocity on the surface following a path that crossed a carbon nanotube at certain angle while the normal and lateral forces were recorded (Figs. 2A–2.,3). Finally, the tip was released from the surface to recover the initial stage (Figs. 2A–2,4). Topographical images of the nanotube were routinely taken before and after the manipulation process. In order to maximize the torsion signal, the manipulation paths were perpendicular to the cantilever. In addition, the carbon nanotubes were selected as perpendicular as possible to the tip path. We also optimized the applied normal force and tip velocity. We used normal force values ranging from 10 to 100 nN and registered the corresponding lateral force curves for each case (Fig. S2). When the normal force was higher than 30 nN the lateral force curve presented an initial step that corresponded to the adherence of the AFM tip at the beginning of the movement due to the friction between the tip and the mica substrate. Once this friction was surpassed, the sliding of the tip along the substrate resulted in a constant lateral force (Figs. 2B and S2). Finally, with a normal force above 80 nN the lateral force reached a plateau. We also explored the effect of the tip velocities when laterally scanning an 11 nm diameter ox-MWCNT adsorbed onto the mica surface (Fig. 2C). We set a normal force of 14 nN low enough to avoid the dragging of the nanotube. The lateral force profiles obtained (Fig. 2C) were similar to the others [47], presenting a peak in the lateral force which corresponded to the maximum friction force between the tip and the nanotube, just before the tip slipped to the other side of the tube. This peak depended on the tip velocity (Fig. 2D) until it reached a plateau at a value around 250 nm/s. Therefore, we chose this value to perform the manipulation experiments.

3.3. Lateral manipulations of nanotubes

We applied the lateral nanomanipulation to ox-MWCNTs and ox-MWCNTS@COF hybrid nanotubes using the optimized normal force (80 nN), a tip path-cantilever angle (90°) and a tip speed value of ~250 nm/s. While the manipulation was performed in contact mode, topographical images of both ox-MWCNTs and ox-MWCNTs@COF

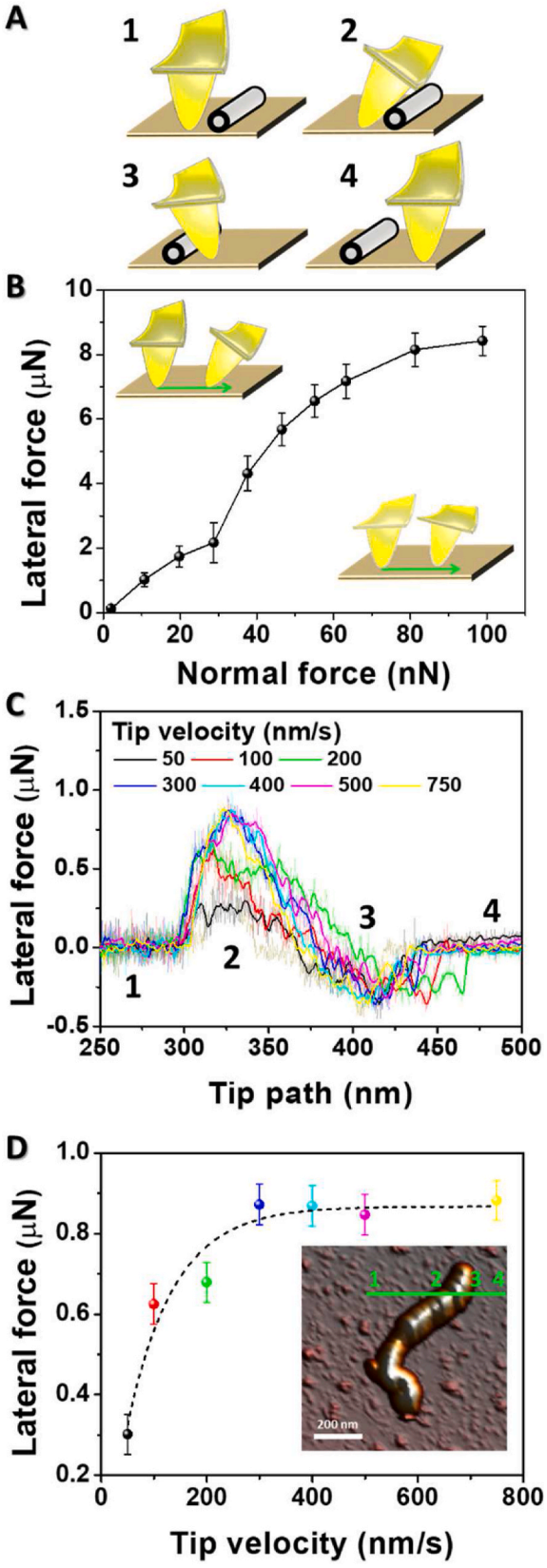

Fig. 2. Manipulation parameters. A) Schematic representation of the AFM tip during lateral scanning of a nanotube. B) Effect of the normal load on the lateral force. C) Lateral force curves and D) Corresponding maximum torsional force as function of the tip velocity. Inset: AFM image of the ox-MWCNT used for the tip velocity test with a green line showing the tip path during manipulation).

nanotubes were acquired in dynamic mode in order to monitor their topographical changes.

A combination of the nanotube topographical images before and after the experiment (Fig. 3A–B, top) with the respective lateral force signals (Fig. 3A–B, bottom) helped to identify the different events along the manipulation procedure for each type of nanotube. Firstly, the lateral force increased when the tip established contact with the tube. In the case of ox-MWCNTs (Fig. 3A), the tip found the nanotube at ~170 nm, and the lateral force increased to 1.85 μN and decreased to 1.08 μN at ~300 nm. The width of this peak (130 nm) coincided with the distance of the bending (Fig. 3A, arrow 2). Afterwards, the lateral force remained constant up to 400 nm, when the tip completed the path and released the tube. This variation of 100 nm coincided with the distance that the tube was displaced at the extreme where bending did not occur (Fig. 3A, arrow 1). Therefore, we proposed that the tube was bent during the lateral force peak and translated without bending at constant force afterwards from 300 nm to 400 nm.

A similar analysis of an ox-MWCNTs@COF tube (Fig. 3B) revealed a constant increment in the lateral force during the distance that the tube was translated and bent (~230 nm, Fig. 3B red arrow). Fig. 3C shows the friction force required to drag the two CNT variants. The thick black curve is the average of seven manipulations performed in seven different ox-MWCNTs. Each thin black curve is the plot for each nanotube. Likewise, the thick and thin red lines are the corresponding plots for eight ox-MWCNTs@COF under similar conditions. In particular, all the lateral manipulations performed on ox-MWCNTs (Fig. 3C, thin black curves) showed similar initial peaks with increments of lateral force up to ~1.5 μN which then decreased and reached a plateau just above ~0.5 μN (Fig. 3C, thick black average curve). By contrast, all ox-MWCNTs@COF data (Fig. 3C, thin red curves) showed a monotonic increase in the force, which reached almost 4 μN until the tip path was completed and the tube was released (Fig. 3, thick red average curve). The area below the curves provides the work of the process, which was calculated for the first 150 nm of the manipulation path, resulting in 90 ± 30 mJ and 280 ± 20 mJ for the ox-MWCNTs and ox-MWCNTs@COF, respectively. Strikingly, the work required to move the hybrid nanotube was ~3 times higher than the ox-MWCNT.

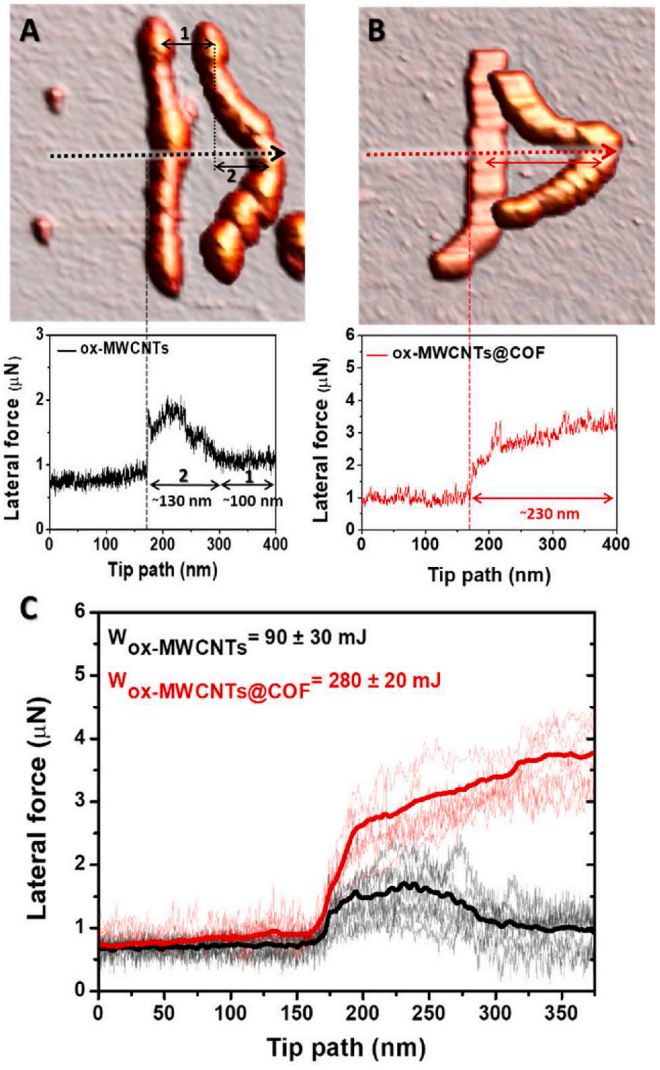

Fig. 3. Single manipulations of tubes. Combination of topographical AFM images of A) ox-MWCNTs and B) ox-MWCNTs@COF nanotubes before and after their manipulation together with their lateral force curves along the tip path (represented with dotted arrows). Inset: Doubled arrows indicate sliding and/or bending events. C) Lateral force curves of 7 and 6 manipulation events for ox-MWCNT (black) and ox-MWCNTs@COF (red) respectively (thin lines). The thick curves show the average data Inset: work of bending calculated by measuring the area below each curve.

The difference between both values revealed that the COF functionalized tubes needed more energy to be slid and/or bent on the surface than the oxidized tubes. While in the case of the ox-MWCNTs, it appears possible to resolve between the bending and sliding events, in the case of the ox-MWCNTs@COF these phenomena appear to be linked and governed by the combination of the tube mechanical properties and the adhesion to the surface. A nanotube resting on a surface with zero adhesion should not bend in order to minimize the elastic energy. However, in this case the curvature of the CNT increased the energy required to sustain this curvature. This energy is provided in the form of adhesion.

The mechanical properties of ox-MWCNT were endorsed with a Young Modulus of 200 GPa [54,55]. By contrast, the COF material used to hybridize with the ox-MWCNTs presented a Young Modulus of 3.17 GPa. [56], which is ~10x lower than the pristine CNT value. Therefore, the bending force should be very similar for both nanotube variants. Consequently, the higher values of lateral force and work needed to deform the ox-MWCNTs@COF on the surface can be explained by these tubes having a larger adhesion force with the mica surface.

In order to further explore this possibility, we performed consecutive lateral manipulations (Figs. 4, S3, S4 and S5) by dragging the same tube several times. An ox-MWCNTs was translated on the surface through 1.5 μm (Fig. 4A) by applying 5 consecutive manipulations. In the first three lateral pushing events (Fig. 4B, red, dark blue and green arrows) the AFM topographies revealed an increased bending of the tube while it was dragged over the mica surface. The lateral force data (Fig. 4B) exhibited similar behaviour to those in Fig. 3C, showing a sudden increase of ~1 μN when the AFM tip established contact with the tube and a decrease afterwards. Beyond showing a small force peak when the tip found the tube, the subsequent lateral pushing (Fig. 4A, light blue and orange arrows) remained almost flat. In fact, the AFM topographies of Fig. 4A show that the results of manipulations 4 (blue) and 5 (orange) hardly changed the shape of the tube and they only dragged the nanotube on the mica surface. This suggests that after manipulation 3, the ox-MWCNTs nanotube had reached its maximum bending state and only slid during the manipulations 4 and 5 (750 nm). These data reveal that ox-MWCNTs sliding occurred under lateral forces of 0.25 μN (Fig. 4B, light blue and orange curves), well below the peaks of ~1 μN exhibited in manipulations 1–3 where bending took place. This fact enabled us to discern between the bending and sliding phenomena in ox-MWCNTs. However, when trying to perform similar manipulation experiments on ox-MWCNTs@COF (Fig. 4C), we achieved the maximum bending state of the tube after two lateral consecutive manipulations of 1.5 μm (red and blue arrows) and then the third manipulation led to the nanotube breaking (green arrow). The lateral force again signalled a monotonic increase (Fig. 4D) up to ~4 μN which corresponded to the combined sliding/bending phenomena of the tube as occurred with the

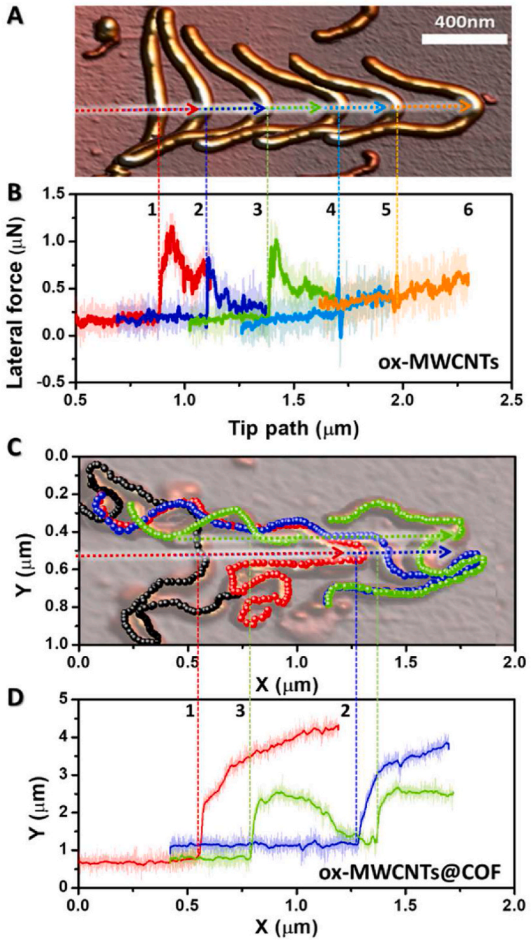

Fig. 4. Sequential manipulations. A) Topographical image reconstructed from the consecutive manipulations of one individual ox-MWCNT nanotube during 5 events. B) Corresponding lateral force curves. C) Cartesian coordinates of ox-MWCNTs@COFs nanotubes during 3 nanomanipulation events merged to topographical images (light colour image). D) Corresponding lateral force curves. Their manipulations are represented with coloured arrows and the positions where the tip finds the nanotube are highlighted by dashed lines in the lateral force curves.

single manipulations in Fig. 3C. However, after reaching its maximum bending state, further manipulations led to the nanotube breaking (green coloured tube, Fig. 4C) instead of sliding as occurred with the ox-MWCNTs. The breaking was observed when the lateral force decreased at 1.2 μm, although it increased again when the rest of the tube was dragged and bent (Fig. 4D, green curve). In other words, the adhesion energy was so high in the ox-MWCNTs@COF that it was much easier to increase the curvature than to induce translation.

The estimation of the torsional work of the consecutive manipulation events (Fig. 5) again resulted in a higher energy in the case of ox-MWCNTs@COF (Fig. 5, red). The last two manipulations of ox-MWCNT only induced the sliding of the tube (Fig. 5, black -4,5-) with an average work of 10 mJ calculated during 150 nm of the path. Therefore, it is possible to subtract this value from the previous bending plus sliding energies (90 mJ, Fig. 5). Following this procedure, we can isolate the bending work in ox-MWCNT for the first three manipulations (Fig. 4A,B), which results in 80 mJ (Fig. 5, black arrows). We stated before that the difference between the CNT and COF Young Modulus implied that the energetic costs of bending ox-MWCNT and ox-MWCNTs@COF are similar. Hence, we can roughly resolve the sliding work of ox-MWCNTs@COF by subtracting the bending energy value of ox-MWCNT from the COF's values (Fig. 5, red arrows). This rough

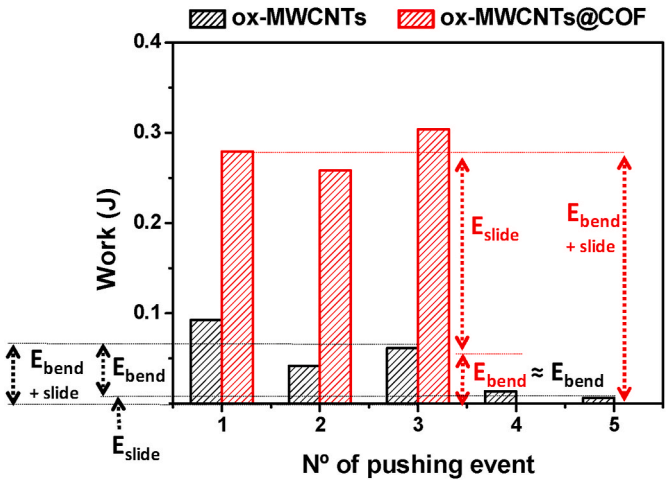

Fig. 5. Work of manipulations. Torsional work calculated for the first 150 nm of consecutive manipulations of Fig. 4 for ox-MWCNTs (separation of bending and sliding) and for ox-MWCNTS@COF (combined bending and sliding). Assuming that the bending of the hybrid should be similar to that of the ox-MWCNTs, the large differences in the work are ascribed to the increased work of sliding in the hybrid.

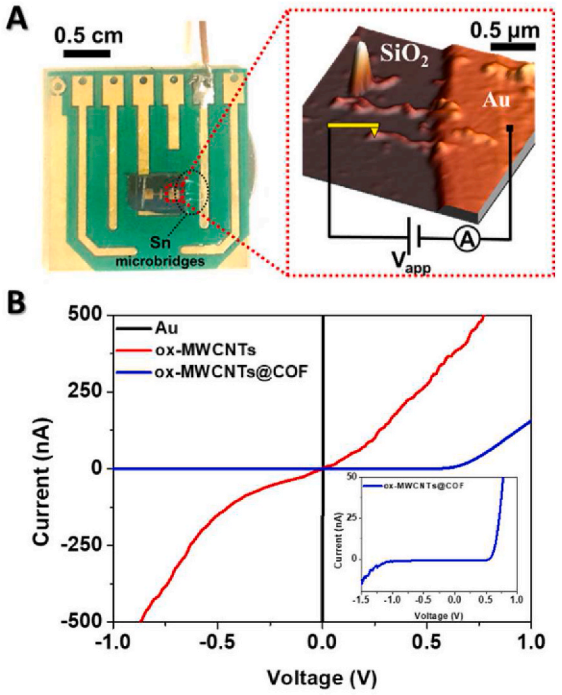

Fig. 6. Electrical transport. A) Set-up used for electrical conductance measurements and AFM image of selected area including the electrical circuit. B) I–V characteristics of gold electrode, ox-MWCNTs and ox-MWCNTs@COF (zoom in the inset).

estimation suggests an average value for the sliding work of 10 mJ and 200 mJ for the ox-MWCNT and ox-MWCNTs@COF tubes, respectively. These values point to an approximately 20 times higher adhesion of the ox-MWCNTs@COF on the mica surface than the ox-MWCNTs. This statement is further supported by the breaking of the COF functionalized tube at the third manipulation (Fig. 4C,D, green): the tube was strongly held by the surface and could only yield by breaking.

The enhanced tube-surface interaction for ox-MWCNTs@COF can be understood by considering the different chemical nature of the tube surfaces. The organic framework used to coat the ox-MWCNTs was

assembled through condensation of amines and aldehydes to form a 3D architecture based on the formation of imine linkages. Therefore, the surface of such material contains aldehyde and amine groups as surface-defective sites. Such organic fragments are very polar and can establish relatively strong dipole-dipole interactions with polar groups of the mica surface or even hydrogen bonding interactions. By contrast, oxygenated fragments in ox-MWCNTs are much less prevalent on its surface, which is characterized by graphenic regions that interact poorly with the mica substrate. These distinctive molecular interactions determine the different adhesion observed for ox-MWCNTs@COF and ox-MWCNTs.

3.4. Electrical measurements of nanotubes

In order to further disclose the physical changes induced by COF on the tubes, we probed their electrical properties. We prepared a set-up (Fig. 6A) by contacting the nanotubes with a pre-evaporated Ti/Au mask which acted as an electrode [57]. Part of the tube was in contact with the gold and then, we used a conductive AFM tip with a Cr–Pt coating (ElectriMulti75-G from BudgetSensors) as a second mobile electrode to establish electrical contact with the uncovered part of the tube. (Fig. 6A, right) [58].

Firstly, we tested the conductive tip on the Ti/Au electrode by approaching the tip to contact and measured ohmic behaviour with a resistance of 5 kΩ (Fig. 6B, black). The current controller provided this minimum contact resistance to prevent a high current that could damage the tips. Subsequently, after stabilising the mechanical contact of the tip with the tube, we applied voltage ramps to measure the tube I–V (intensity current *vs*. voltage) responses (Fig. 6B) [58]. The ox-MWCNT has a near-ohmic I–V (Fig. 6B, red) with a resistance of ~0.3 MΩ which accounts for the existence of different electronic characteristic tubes (metallic and semiconductor) within the ox-MWCNT structure [57]. This electrical behaviour was deeply altered with COF functionalization (Fig. 6B, blue), presenting a non-linear and asymmetric rectifying behaviour with a resistance of ~3.3 MΩ. This resistance value corresponded to the slope when the current started to increase at voltages higher than 0.5 V. The current flow was enabled at a voltage higher than 0.5 V as could be seen by the high current increase whereas it was blocked between −1 and 0.5 V. For the lower voltages, a very small increase in current could be observed (Fig. 6D, inset).

These results are consistent with metallic-semiconductor junctions (p-n diodes) formed at the interface of two constituents [59]. In fact, in the case of this hybrid, the imine linkages of the COF material form an extended electron-rich conjugated system, rendering to a p-type semiconducting behaviour [60], which can facilitate the formation of a Schottky junction at the interface with the ox-MWCNTs, which finally enables the electron transport with high mobility [61,62].

4. Conclusions

We used AFM to manipulate ox-MWCNTs and a hybrid ox-MWCNTs@COF adsorbed on a mica surface by performing lateral force curves. This work demonstrates that the presence of a COF layer modifies the properties of the nanotube surface with two consequences. Firstly, the tribological response of this new hybrid nanotube (ox-MWCNTs@COF) compared with that of ox-MWCNTs results in an adhesion of ox-MWCNTs@COF of about 20 times higher than the ox-MWCNT. Secondly, the change in the surface properties of nanotubes as a result of the COF coating was also observed when the electric conductivity was studied at the nanoscale. For this purpose, we used a conductive AFM tip as a mobile electrode to determine the electronic transport of the oxidized MWCNTs and the ox-MWCNTs@COF hybrids. These experiments have demonstrated that the ox-MWCNTs@COF hybrids exhibit a lower conductivity than their ox-MWCNTs counterparts and they present rectifying behaviour and they present rectifying behaviour. These observations can have a significant impact on the use of CNT's in nanoelectronic devices. These results open up the possibility of being able to fine-tune the mechanical and electrical properties of the nanotubes from their synthesis which is very relevant in the development of applications such as field-effect transistors (FETs) or ambipolar and n-type nanotube transistors).

CRediT authorship contribution statement

Alicia Moya: Investigation, Conceptualization, Data curation, Validation, Methodology, Formal analysis, Writing - original draft, Writing - review & editing. **José Alemán:** Resources. **Julio Gómez-Herrero:** Methodology, Resources. **Rubén Mas-Ballesté:** Data curation, Supervision, Writing - review & editing. **Pedro J. de Pablo:** Conceptualization, Data curation, Funding acquisition, Methodology, Project administration, Validation, Supervision, Validation, Resources, Methodology, Writing - review & editing.

Declaration of competing interest

The authors declare that they have no known competing financial interests or personal relationships that could have appeared to influence the work reported in this paper.

Acknowledgements

P. J.d.P. acknowledges support by grants from the Ministerio de Ciencia e Innovación (FIS2017- 89549-R; "Maria de Maeztu" Program for Units of Excellence in R&D MDM2014-0377; and FIS2017-90701-REDT) and the Human Frontiers Science Program (HFSPO RGP0012/2018). R. M. ackowledges support by grant PID2019-110637RB-100.

Appendix A. Supplementary data

Supplementary data to this article can be found online at https://doi.org/10.1016/j.carbon.2022.07.053.

References

[1] J.-P. Salvetat, J.-M. Bonard, N.H. Thomson, A.J. Kulik, L. Forró, W. Benoit, L. Zuppiroli, Mechanical properties of carbon nanotubes, Appl. Phys. A 69 (1999) 255–260, https://doi.org/10.1007/s003390050999.
[2] B. Peng, M. Locascio, P. Zapol, S. Li, S.L. Mielke, G.C. Schatz, H.D. Espinosa, Measurements of near-ultimate strength for multiwalled carbon nanotubes and irradiation-induced crosslinking improvements, Nat. Nanotechnol. 3 (2008) 626, https://doi.org/10.1038/nnano.2008.211.
[3] A. Lekawa-Raus, J. Patmore, L. Kurzepa, J. Bulmer, K. Koziol, Electrical properties of carbon nanotube based fibers and their future use in electrical wiring, Adv. Funct. Mater. 24 (2014) 3661–3682, https://doi.org/10.1002/adfm.201303716.
[4] A.A. Balandin, Thermal properties of graphene and nanostructured carbon materials, Nat. Mater. 10 (2011) 569, https://doi.org/10.1038/nmat3064.
[5] J.-M. Bonard, H. Kind, T. Stöckli, L.-O. Nilsson, Field emission from carbon nanotubes: the first five years, Solid State Electron. 45 (2001) 893–914, https://doi.org/10.1016/S0038-1101(00)00213-6.
[6] V. Sgobba, D.M. Guldi, Carbon nanotubes as integrative materials for organic photovoltaic devices, J. Mater. Chem. 18 (2008) 153–157, https://doi.org/10.1039/B713798M.
[7] G. Wang, L. Zhang, J. Zhang, A review of electrode materials for electrochemical supercapacitors, Chem. Soc. Rev. 41 (2012) 797–828, https://doi.org/10.1039/C1CS15060J.
[8] Y. Wu, J. Wang, K. Jiang, S. Fan, Applications of carbon nanotubes in high performance lithium ion batteries, Front. Phys. 9 (2014) 351–369, https://doi.org/10.1007/s11467-013-0308-x.
[9] A. Peigney, Ch Laurent, E. Flahaut, R.R. Bacsa, A. Rousset, Specific surface area of carbon nanotubes and bundles of carbon nanotubes, Carbon 39 (2001) 507–514, https://doi.org/10.1016/S0008-6223(00)00155-X.
[10] J.J. Vilatela, D. Eder, Nanocarbon composites and hybrids in sustainability: a review (ChemSusChem 3/2012), ChemSusChem 5 (2012), https://doi.org/10.1002/cssc.201290009, 441–441.
[11] D. Eder, Carbon Nanotube–Inorganic hybrids, Chem. Rev. 110 (2010) 1348–1385, https://doi.org/10.1021/cr800433k.
[12] N.A.M. Noor, J.A. Razak, S. Ismail, N. Mohamad, L.K. Tee, R.F. Munawar, R. Junid, Review on carbon nanotube based polymer composites and its applications, J. Adv. Manuf. Technol. 12 (1970). https://jamt.utem.edu.my/jamt/article/view/4018. (Accessed 2 June 2020).

[13] J.C. Anike, K. Belay, J.L. Abot, Effect of twist on the electromechanical properties of carbon nanotube yarns, Carbon 142 (2019) 491–503, https://doi.org/10.1016/j.carbon.2018.10.067.

[14] J. Cao, Q. Wang, H. Dai, Electromechanical properties of metallic, quasimetallic, and semiconducting carbon nanotubes under stretching, Phys. Rev. Lett. 90 (2003), 157601, https://doi.org/10.1103/PhysRevLett.90.157601.

[15] X. Zang, Q. Zhou, J. Chang, Y. Liu, L. Lin, Graphene and carbon nanotube (CNT) in MEMS/NEMS applications, Microelectron. Eng. 132 (2015) 192–206, https://doi.org/10.1016/j.mee.2014.10.023.

[16] M. Moreno-Moreno, P. Ares, C. Moreno, F. Zamora, C. Gómez-Navarro, J. Gómez-Herrero, AFM manipulation of gold nanowires to build electrical circuits, Nano Lett. 19 (2019) 5459–5468, https://doi.org/10.1021/acs.nanolett.9b01972.

[17] H. Xie, D.S. Haliyo, S. Régnier, A versatile atomic force microscope for three-dimensional nanomanipulation and nanoassembly, Nanotechnology 20 (2009), 215301, https://doi.org/10.1088/0957-4484/20/21/215301.

[18] M. Marrese, V. Guarino, L. Ambrosio, Atomic force microscopy: a powerful tool to address scaffold design in tissue engineering, J. Funct. Biomater. 8 (2017) 7, https://doi.org/10.3390/jfb8010007.

[19] T. Hertel, R. Martel, P. Avouris, Manipulation of individual carbon nanotubes and their interaction with surfaces, J. Phys. Chem. B 102 (1998) 910–915, https://doi.org/10.1021/jp9734686.

[20] S. Wu, X. Fu, X. Hu, X. Hu, Manipulation and behavior modeling of one-dimensional nanomaterials on a structured surface, Appl. Surf. Sci. 256 (2010) 4738–4744, https://doi.org/10.1016/j.apsusc.2010.02.084.

[21] S.-C. Yang, X. Qian, Controlled manipulation of flexible carbon nanotubes through shape-dependent pushing by atomic force microscopy, Langmuir 29 (2013) 11793–11801, https://doi.org/10.1021/la401939j.

[22] M.C. Strus, R.R. Lahiji, P. Ares, V. López, A. Raman, R. Reifenberger, Strain energy and lateral friction force distributions of carbon nanotubes manipulated into shapes by atomic force microscopy, Nanotechnology 20 (2009), 385709, https://doi.org/10.1088/0957-4484/20/38/385709.

[23] M. Bordag, A. Ribayrol, G. Conache, L.E. Fröberg, S. Gray, L. Samuelson, L. Montelius, H. Pettersson, Shear stress measurements on InAs nanowires by AFM manipulation, Small 3 (2007) 1398–1401, https://doi.org/10.1002/smll.200700052.

[24] G. Conache, S.M. Gray, A. Ribayrol, L.E. Fröberg, L. Samuelson, H. Pettersson, L. Montelius, Friction measurements of InAs nanowires on silicon nitride by AFM manipulation, Small 5 (2009) 203–207, https://doi.org/10.1002/smll.200800794.

[25] E. Gnecco, A. Rao, K. Mougin, G. Chandrasekar, E. Meyer, Controlled manipulation of rigid nanorods by atomic force microscopy, Nanotechnology 21 (2010), 215702, https://doi.org/10.1088/0957-4484/21/21/215702.

[26] Q. Qin, Y. Zhu, Static friction between silicon nanowires and elastomeric substrates, ACS Nano 5 (2011) 7404–7410, https://doi.org/10.1021/nn202343w.

[27] J.-H. Hsu, S.-H. Chang, Tribological interaction between multi-walled carbon nanotubes and silica surface using lateral force microscopy, Wear 266 (2009) 952–959, https://doi.org/10.1016/j.wear.2008.12.017.

[28] H.-J. Kim, K.H. Kang, D.-E. Kim, Sliding and rolling frictional behavior of a single ZnO nanowire during manipulation with an AFM, Nanoscale 5 (2013) 6081–6087, https://doi.org/10.1039/C3NR34029E.

[29] X. Zeng, Y. Peng, H. Lang, X. Cao, Nanotribological behavior of a single silver nanowire on graphite, Nanotechnology 29 (2018), 085706, https://doi.org/10.1088/1361-6528/aaa2e5.

[30] M. Zheng, X. Chen, C. Park, C.C. Fay, N.M. Pugno, C. Ke, Nanomechanical cutting of boron nitride nanotubes by atomic force microscopy, Nanotechnology 24 (2013), 505719, https://doi.org/10.1088/0957-4484/24/50/505719.

[31] H.-J. Kim, G.H. Nguyen, D.L.C. Ky, D.K. Tran, K.-J. Jeon, K.-H. Chung, Static and kinetic friction characteristics of nanowire on different substrates, Appl. Surf. Sci. 379 (2016) 452–461, https://doi.org/10.1016/j.apsusc.2016.04.097.

[32] S. Kumar, I. Kaur, N. Kumari, S. Jain, K. Dharamveer, V.K. Jindal, N.K. Verma, L. M. Bharadwaj, Atomic force microscope manipulation of multiwalled and single walled carbon nanotubes with reflux and ultrasonic treatments, Appl. Nanosci. 4 (2014) 19–26, https://doi.org/10.1007/s13204-012-0166-9.

[33] M.R. Falvo, R.M. Taylor II, A. Helser, V. Chi, F.P. Brooks Jr., S. Washburn, R. Superfine, Nanometre-scale rolling and sliding of carbon nanotubes, Nature 397 (1999) 236, https://doi.org/10.1038/16662.

[34] A. Moya, A. Cherevan, S. Marchesan, P. Gebhardt, M. Prato, D. Eder, J.J. Vilatela, Oxygen vacancies and interfaces enhancing photocatalytic hydrogen production in mesoporous CNT/TiO2 hybrids, Appl. Catal. B Environ. 179 (2015) 574–582, https://doi.org/10.1016/j.apcatb.2015.05.052.

[35] S. Grau, S. Berardi, A. Moya, R. Matheu, V. Cristino, J.J. Vilatela, C.A. Bignozzi, S. Caramori, C. Gimbert-Suriñach, A. Llobet, A hybrid molecular photoanode for efficient light-induced water oxidation, Sustain. Energy Fuels 2 (2018), https://doi.org/10.1039/C8SE00146D, 1979–1985.

[36] D. Tasis, N. Tagmatarchis, A. Bianco, M. Prato, Chemistry of carbon nanotubes, Chem. Rev. 106 (2006) 1105–1136, https://doi.org/10.1021/cr050569o.

[37] J.W. Colson, A.R. Woll, A. Mukherjee, M.P. Levendorf, E.L. Spitler, V.B. Shields, M. G. Spencer, J. Park, W.R. Dichtel, Oriented 2D covalent organic framework thin films on single-layer graphene, Science 332 (2011) 228, https://doi.org/10.1126/science.1202747.

[38] J. Yoo, S.-J. Cho, G.Y. Jung, S.H. Kim, K.-H. Choi, J.-H. Kim, C.K. Lee, S.K. Kwak, S.-Y. Lee, COF-net on CNT-net as a molecularly designed, hierarchical porous chemical trap for polysulfides in lithium–sulfur batteries, Nano Lett. 16 (2016) 3292–3300, https://doi.org/10.1021/acs.nanolett.6b00870.

[39] J. Yoo, S. Lee, S. Hirata, C. Kim, C.K. Lee, T. Shiraki, N. Nakashima, J.K. Shim, In situ synthesis of covalent organic frameworks (COFs) on carbon nanotubes and graphenes by sonochemical reaction for CO2 adsorbents, Chem. Lett. 44 (2015) 560–562, https://doi.org/10.1246/cl.141194.

[40] B. Sun, J. Liu, A. Cao, W. Song, D. Wang, Interfacial synthesis of ordered and stable covalent organic frameworks on amino-functionalized carbon nanotubes with enhanced electrochemical performance, Chem. Commun. 53 (2017) 6303–6306, https://doi.org/10.1039/C7CC01902E.

[41] A. Moya, M. Hernando-Pérez, M. Pérez-Illana, C. San Martín, J. Gómez-Herrero, J. Alemán, R. Mas-Ballesté, P.J. de Pablo, Multifunctional carbon nanotubes covalently coated with imine-based covalent organic frameworks: exploring structure–property relationships through nanomechanics, Nanoscale 12 (2020) 1128–1137, https://doi.org/10.1039/C9NR07716B.

[42] P.J. de Pablo, J. Colchero, M. Luna, J. Gómez-Herrero, A.M. Baró, Tip-sample interaction in tapping-mode scanning force microscopy, Phys. Rev. B 61 (2000) 14179–14183, https://doi.org/10.1103/PhysRevB.61.14179.

[43] J.E. Sader, J.W.M. Chon, P. Mulvaney, Calibration of rectangular atomic force microscope cantilevers, Rev. Sci. Instrum. 70 (1999) 3967–3969, https://doi.org/10.1063/1.1150021.

[44] I. Horcas, R. Fernández, J.M. Gómez-Rodríguez, J. Colchero, J. Gómez-Herrero, A. M. Baro, WSXM: a software for scanning probe microscopy and a tool for nanotechnology, Rev. Sci. Instrum. 78 (2007), 013705, https://doi.org/10.1063/1.2432410.

[45] M. Varenberg, I. Etsion, G. Halperin, An improved wedge calibration method for lateral force in atomic force microscopy, Rev. Sci. Instrum. 74 (2003) 3362–3367, https://doi.org/10.1063/1.1584082.

[46] R.J. Cannara, M. Eglin, R.W. Carpick, Lateral force calibration in atomic force microscopy: a new lateral force calibration method and general guidelines for optimization, Rev. Sci. Instrum. 77 (2006), 053701, https://doi.org/10.1063/1.2198768.

[47] J. Lievonen, M. Ahlskog, Lateral force microscopy of multiwalled carbon nanotubes, Ultramicroscopy 109 (2009) 825–829, https://doi.org/10.1016/j.ultramic.2009.03.028.

[48] P. Avouris, T. Hertel, R. Martel, T. Schmidt, H.R. Shea, R.E. Walkup, Carbon nanotubes: nanomechanics, manipulation, and electronic devices, Appl. Surf. Sci. 141 (1999) 201–209, https://doi.org/10.1016/S0169-4332(98)00506-6.

[49] J. Colchero, Force calibration, in: Procedures in Scanning Probe Microscopy, John Wiley & Sons, Ltd, 1998, pp. 133–1638.

[50] Jaime Colchero, Reibungskraftmikroskopie, Universität Konstanz, 1993.

[51] Calibration grating, Https://Tipsnano.Com/Catalog/Calibration/Tgs1/. (n.d.), https://tipsnano.com/catalog/calibration/tgs1/.

[52] J. Yu, N. Grossiord, C.E. Koning, J. Loos, Controlling the dispersion of multi-wall carbon nanotubes in aqueous surfactant solution, Carbon 45 (2007) 618–623, https://doi.org/10.1016/j.carbon.2006.10.010.

[54] X. Liu, J. Luo, J. Fan, S. Lin, L. Jia, X. Jia, Q. Cai, X. Yang, Comprehensive enhancement in overall properties of MWCNTs-COOH/epoxy composites by microwave: an efficient approach to strengthen interfacial bonding via localized superheating effect, Compos. B Eng. 174 (2019), 106909, https://doi.org/10.1016/j.compositesb.2019.106909.

[55] R.S. Ruoff, D. Qian, W.K. Liu, Mechanical properties of carbon nanotubes: theoretical predictions and experimental measurements, Compt. Rendus Phys. 4 (2003) 993–1008, https://doi.org/10.1016/j.crhy.2003.08.001.

[56] B. Lukose, A. Kuc, T. Heine, Stability and electronic properties of 3D covalent organic frameworks, J. Mol. Model. 19 (2013) 2143–2148, https://doi.org/10.1007/s00894-012-1671-1.

[57] P.J. de Pablo, E. Graugnard, B. Walsh, R.P. Andres, S. Datta, R. Reifenberger, A simple, reliable technique for making electrical contact to multiwalled carbon nanotubes, Appl. Phys. Lett. 74 (1999) 323–325, https://doi.org/10.1063/1.123011.

[58] P.J. de Pablo, C. Gómez-Navarro, M.T. Martínez, A.M. Benito, W.K. Maser, J. Colchero, J. Gómez-Herrero, A.M. Baró, Performing current versus voltage measurements of single-walled carbon nanotubes using scanning force microscopy, Appl. Phys. Lett. 80 (2002) 1462–1464, https://doi.org/10.1063/1.1453475.

[59] M. Xiao, S. Zheng, D. Shen, W.W. Duley, Y.N. Zhou, Laser-induced joining of nanoscale materials: processing, properties, and applications, Nano Today 35 (2020), 100959, https://doi.org/10.1016/j.nantod.2020.100959.

[60] L. Yang, D.-C. Wei, Semiconducting covalent organic frameworks: a type of two-dimensional conducting polymers, Chin. Chem. Lett. 27 (2016) 1395–1404, https://doi.org/10.1016/j.cclet.2016.07.010.

[61] J. Svensson, E.E.B. Campbell, Schottky barriers in carbon nanotube-metal contacts, J. Appl. Phys. 110 (2011), 111101, https://doi.org/10.1063/1.3664139.

[62] A. Saha, A. Moya, A. Kahnt, D. Iglesias, S. Marchesan, R. Wannemacher, M. Prato, J.J. Vilatela, D.M. Guldi, Interfacial charge transfer in functionalized multi-walled carbon nanotube@TiO2 nanofibres, Nanoscale 9 (2017) 7911–7921, https://doi.org/10.1039/C7NR00759K.